SANDIA REPORT

SAND2010-6203
Unlimited Release
Printed September 2010

Uncertainty Quantification for Large-Scale Ocean Circulation Predictions

Cosmin Safta, Khachik Sargsyan, Bert Debusschere, Habib Najm

Prepared by
Sandia National Laboratories
Albuquerque, New Mexico 87185 and Livermore, California 94550

Sandia National Laboratories is a multi-program laboratory managed and operated by Sandia Corporation, a wholly owned subsidiary of Lockheed Martin Corporation, for the U.S. Department of Energy's National Nuclear Security Administration under contract DE-AC04-94AL85000.

Issued by Sandia National Laboratories, operated for the United States Department of Energy by Sandia Corporation.

Available to DOE and DOE contractors from
U.S. Department of Energy
Office of Scientific and Technical Information
P.O. Box 62
Oak Ridge, TN 37831

Telephone: (865) 576-8401
Facsimile: (865) 576-5728
E-Mail: reports@adonis.osti.gov
Online ordering: http://www.osti.gov/bridge

Available to the public from
U.S. Department of Commerce
National Technical Information Service
5285 Port Royal Rd
Springfield, VA 22161

Telephone: (800) 553-6847
Facsimile: (703) 605-6900
E-Mail: orders@ntis.fedworld.gov
Online ordering: http://www.ntis.gov/help/ordermethods.asp?loc=7-4-0#online

SAND2010-6203
Unlimited Release
Printed September 2010

Uncertainty Quantificatio for Large-Scale Ocean Circulation Predictions

Cosmin Safta, Khachik Sargsyan, Bert Debusschere, Habib Najm
Sandia National Laboratories, P.O. Box 969, Livermore, CA, 94551-0969
{csafta,ksargsy,bjdebus,hnnajm}@sandia.gov

Abstract

Uncertainty quantificatio in climate models is challenged by the sparsity of the available climate data due to the high computational cost of the model runs. Another feature that prevents classical uncertainty analyses from being easily applicable is the bifurcative behavior in the climate data with respect to certain parameters. A typical example is the Meridional Overturning Circulation in the Atlantic Ocean. The maximum overturning stream function exhibits discontinuity across a curve in the space of two uncertain parameters, namely climate sensitivity and CO_2 forcing. We develop a methodology that performs uncertainty quantificatio in the presence of limited data that have discontinuous character. Our approach is two-fold. First we detect the discontinuity location with a Bayesian inference, thus obtaining a probabilistic representation of the discontinuity curve location in presence of arbitrarily distributed input parameter values. Furthermore, we developed a spectral approach that relies on Polynomial Chaos (PC) expansions on each sides of the discontinuity curve leading to an averaged-PC representation of the forward model that allows efficien uncertainty quantificatio and propagation. The methodology is tested on synthetic examples of discontinuous data with adjustable sharpness and structure.

Acknowledgment

This work was supported by Sandia National Laboratories Seniors' Council LDRD (Laboratory Directed Research and Development) program. Sandia National Laboratories is a multi-program laboratory operated by Sandia Corporation, a wholly owned subsidiary of Lockheed Martin Company, for the U.S. Department of Energy's National Nuclear Security Administration under contract DE-AC04-94AL85000.

Contents

List of Figures

This page intentionally left blank.

Chapter 1

Executive Summary

Recent advances in computational capabilities have boosted algorithmic development efforts in uncertainty quantif cation of complex physical models. In order to properly characterize uncertainties in the model outputs, the most intuitively clear approach relies on Monte Carlo (MC) sampling of the inputs. However, even with the substantial computational power of modern computers, the MC approach remains ineff cient due to its slow convergence rate, i.e. one typically needs too many forward model simulations in order to accurately characterize output uncertainties. In this regard, spectral expansions [9, 14] provide a more eff cient approach that allows eff cient uncertainty quantif cation employing compact representation of the output with respect to a spectral basis functions of random variables. In this work we will employ Polynomial Chaos (PC) expansions to represent input parameters and output observables with respect to standard (Legendre) polynomial bases of input arguments that are standard (uniform) random variables. We focus on a non-intrusive approach, where the forward model is used as a black-box and is only evaluated at sampled input parameter conf gurations in order to obtain a spectral representation. The PC expansions, while retaining the probabilistic information, represent the input-output relationship using a set of deterministic numbers, PC coeff cients or PC modes. The basis orthogonality allows Fourier-like projection formulae for these modes. However, this orthogonal projection requires the forward model runs to be taken at specif c, pre-determined parameter values. Often, the forward model runs are too expensive or are given apriori, hence this restriction becomes handicap. For this reason we also employ Bayesian inference as an alternative approach to determine the PC modes. This approach, although is generically less precise than the orthogonal projection, allows obtaining a compact PC representation and associated posterior uncertainties without restricting the input parameter locations at which the forward model is evaluated. In cases where extra forward model runs are possible, we suggest using a hybrid approach that balances between the accuracy of the quadrature projection approach and the f exibility of the Bayesian inference.

This page intentionally left blank.

Chapter 2

Introduction

This work has been motivated by the climate modeling community, since the climate models often exhibit discontinuous behavior with respect to various input parameters. At the same time, the climate models are extremely complex, hence one can afford only limited number of model runs. Because of limited observations and the difficulties associated with high-resolution modeling, the current state of predictive power is quite restricted, necessitating the need to account for uncertainty in climate models and associated model parameters. For example, consider the *Meridional Overturning Circulation* (MOC), as one of the most discussed environmental phenomena that can potentially collapse [24] as a result of increased greenhouse gas concentrations. In the MOC, warm surface currents transport heat from the tropics northward while deep cold water masses from the North Atlantic flow to warmer ocean basins. The MOC plays an extremely important role in the northward heat transport in the Atlantic Ocean [8] and its weakening or collapse would cause major climatic change and, consequently, economic disruptions. Many studies suggest that the atmospheric CO_2 increase will damage the MOC significantly, and a potential collapse of the circulation is possible. The rate of CO_2 increase, denoted by r, is one of the most important parameters in MOC modeling, together with the climate sensitivity (λ) parameter, defined as the equilibrium change in the temperature that corresponds to a hypothetical doubling of the atmospheric CO_2 concentration. Evidence from paleoclimatic reconstructions [18] and from recent model simulations reveals that MOC behavior exhibits a bifurcation with respect to the pair of parameters (λ, r). Namely, the MOC collapses as the parameters cross a curve $r = \tilde{r}(\lambda)$ in the parametric (λ, r) space. In recent papers [30, 26], a detailed analysis of the MOC dependence on the two parameters r and λ has been carried out. The authors use a forward model of intermediate complexity that consists of a three-dimensional global circulation model (GCM) coupled with both a zonally averaged atmospheric and a thermodynamic sea-ice model. A single run of a time span of a couple of centuries can take several weeks to simulate on a supercomputer. Webster *et al.* [30] explore the uncertainty in the MOC as a function of two uncertain parameters λ and r, each characterized by a probability distribution function. However, the computational cost of the forward model restricts the uncertainty quantification analysis, since only a small number of sampling runs are plausible. By obtaining simulation data on maximum overturning circulation in the North Atlantic from a small number of hypothetical pairs of parameters, the response surface is then constructed using the Deterministic Equivalent Modeling Method (DEMM) [29, 31]. It relies on the expansion of the response in terms of global orthogonal polynomials, and therefore is bound to fail in case of bifurcations, since no linear combination of polynomials can properly represent a discontinuous response function. Although eventually the authors achieved a reasonable representation of the response surface by using ad-hoc information about the structure of the response,

they recognized the necessity of determining the response surface characteristics in a more general manner, as well as the importance of identifying optimal sampling points *prior* to the simulations.

Given the clearly recognized need for uncertainty analysis in forward predictive modeling, we outline and tackle two major issues: (a) the need to represent model output in a (problem-independent) fashion that takes into account bifurcations/discontinuities and (b) the need to perform uncertainty quantification with only a limited set of sample points, due to the computational cost of the forward model. Hence, here and thereafter, by referring to the sparsity of the data we mean the computational challenges associated with obtaining the data from a complicated forward model.

It is well-recognized [9] that the global polynomial-based spectral expansions have an inherent assumption of smoothness of the output with respect to input parameters. Otherwise, when the forward model data exhibits a discontinuity across a certain region in the parameter space, these expansions are not precise enough (at low orders) or suffer from the Gibbs phenomenon (at high orders). One approach to circumvent the discontinuity problem is to enrich the basis by a function of discontinuous form. The basis enrichment approach has been borrowed from the finite elements community and successfully applied in [5, 6, 21, 10]. The method however requires precise knowledge of the discontinuity location, and hence is infeasible in many contexts. Another approach is to use local spectral expansions that rely on - often adaptive - domain decompositions of the parameter space [13, 15, 16]. These methods were used, for example, to characterize problems with bifurcative convective [17] and chemical [20] structure. However, this approach requires new forward model runs at each refinement step. This can quickly - after a couple of domain splits - become computationally too costly for complex forward models.

Discontinuity or edge detection algorithms form an important component in many fields, e.g. climate change research, image recognition, or digital signal processing [32, 3, 30]. However, they often require input parameters to be sampled at a uniform grid, and lead to a single answer, while, clearly, when only limited data is available, a probabilistic representation should be preferred. Also, the classical edge detection algorithms are fine-tuned to the two-dimensional case for proper image processing, and do not scale well to higher dimensions. Discontinuity detection in the context of uncertainty analysis has been performed in [2], where authors proposed a polynomial fitting technique for one- and two-dimensional fields and then further extended the methodology to multivariate stochastic spaces [1]. This approach relies on the global polynomial chaos coefficients and relies on function evaluations on rectangular grids to determine the location of jump discontinuities. Another approach to tackle the issues associated with discontinuities in forward model runs is based on Padé-Legendre interpolants. For example, Chantrasmi *et al.* [4] proposed a non-intrusive uncertainty propagation methodology for problems with highly nonlinear or discontinuous responses using Padé-Legendre interpolants. However, this methodology also relies on the forward model being simulated at a rectangular grid to enable corresponding integral computations.

Our approach for detecting discontinuities can be viewed as independent from the rest of the spectral methodology, and leads to a probabilistic answer for the discontinuity location given limited number of forward model evaluations at arbitrary parameter values, without any conceptual handicaps towards high-dimensional generalization. The methodology propose here is essentially

a "smarter" domain decomposition, and is two-fold: first we locate the discontinuity using a Bayesian inference approach, and then we split the parameter domain into two pieces and apply PC methods on each side of the discontinuity. In order to preserve the desirable orthogonality properties of the basis functions, we apply a Rosenblatt transformation to map domains from each side of the discontinuity to rectangular ones. Moreover, since our approach of discontinuity detection is Bayesian, it allows for uncertainty characterization of the discontinuity location, hence we can average over the distribution of these discontinuity curves, thus obtaining an averaged-PC expansion that compactly represents the input-output relationship. This representation can serve as a surrogate forward model to help propagate input uncertainties efficiently through the model, or for inverse problems that require many forward model runs.

This report is organized as follows. The discontinuity detection algorithm is introduced and tested in Section 3. The global PC construction is described in Section 4, including subsections detailing the orthogonal projection approach, the Bayesian inference approach and the failure of the global methodology on discontinuous data. Then, Section 5 introduces the 'smart' domain decomposition approach coupled with PC expansion, as well as illustrates the full uncertainty propagation algorithm on a test case. We then finish the paper with discussion of the results and future work in Section 6.

This page intentionally left blank.

Chapter 3

Bayesian Inference of the Discontinuity Location

We propose a methodology that infers a discontinuity in the forward model given f nitely many, and generally a small number of evaluations of the model. After appropriately parameterizing the discontinuity curve, the algorithm employs Bayesian inference to f nd a probabilistic description of the curve parameters.

For clarity, let us focus on a two-dimensional case, since generalization to multidimensional data is straightforward. Also, assume the model $Z(\lambda) = Z(\lambda_1, \lambda_2) : I_{\lambda_1} \times I_{\lambda_2} \to \mathbb{R}$ changes sharply as the arguments cross a smooth curve $G(\lambda_1, \lambda_2) = 0$, and the input parameters belong to intervals $I_{\lambda_1}, I_{\lambda_2} \subset \mathbb{R}$. Assume N values $\{z_i\}_{i=1}^N$ of the forward model at points $\{\lambda_i\}_{i=1}^N \subset I_{\lambda_1} \times I_{\lambda_2}$ are available.

We parameterize the, yet unknown, discontinuity curve $G(\lambda_1, \lambda_2) = 0$ as a polynomial function $\lambda_2 = p_C(\lambda_1)$ of order K.

$$\lambda_2 = p_C(\lambda_1) = \sum_{k=0}^{K} c_k \lambda_1^k. \tag{3.1}$$

Our goal is to infer the coeff cients $c = (c_0, \ldots, c_K)$ of the polynomial $p_C(\cdot)$.

The assumption that λ_1 and λ_2 on the discontinuity curve are related through a single-valued function (3.1) can be lifted by parameterizing the discontinuity curve $G(\lambda_1, \lambda_2) = 0$ along, say, its length s, i.e. $\lambda_1 = \lambda_1(s)$, $\lambda_2 = \lambda_2(s)$. However, we will keep the simple polynomial assumption (3.1) for the clarity of presentation. In principle, the discontinuity location expansion (3.1) can be parameterized using some prior information about its features. Given the lack of any prior knowledge in the present context, we use a polynomial parameterization. Next, we describe the Bayesian algorithm that infers the coeff cients $c = (c_0, \ldots, c_K)$ of the polynomial $\lambda_2 = p_C(\lambda_1)$.

Bayes' formula for the posterior probability of Model $\mathcal{M}$ given the Data $\mathcal{D} = \{z_1, \ldots, z_N\}$ is

$$P(\mathcal{M}\,|\mathcal{D}) = \frac{P(\mathcal{D}\,|\mathcal{M})P(\mathcal{M})}{P(\mathcal{D})}, \tag{3.2}$$

where the prior probability $P(\mathcal{M})$ and the posterior probability $P(\mathcal{M}\,|\mathcal{D})$ represent degrees of belief about Model $\mathcal{M}$, before and after having the particular Data $\mathcal{D}$, respectively [28]. The likelihood function, viewed as a function of the Model, $L(\mathcal{M}) = P(\mathcal{D}\,|\mathcal{M})$ represents the probability

of obtaining the data set $\mathcal{D}$ *if* it was drawn from the Model $\mathcal{M}$. The *evidence* $P(\mathcal{D})$ is the same probability, marginalized over $\mathcal{M}$ and, in the Bayesian algorithms below, simply plays the role of a normalizing constant. We presume a simplif ed approximation model for the function $Z(\lambda_1,\lambda_2)$ as a hyperbolic tangent function between limiting values m_L and m_R with steepness parameter α and discontinuity along the postulated K-th order polynomial $\lambda_2 = p_C(\lambda_1) = \sum_{k=0}^{K} c_k \lambda_1^k$:

$$\mathcal{M}_C \equiv g(\lambda_1,\lambda_2) = m_L \frac{1-\tanh\left(\alpha(\lambda_2 - p_C(\lambda_1))\right)}{2} + m_R \frac{1+\tanh\left(\alpha(\lambda_2 - p_C(\lambda_1))\right)}{2}. \tag{3.3}$$

In order to construct the likelihood function, for each pair (λ_1,λ_2) we assume a zero-mean Gaussian statistical noise model for the discrepancy between the simplif ed model (3.3) and the data. The variance of the noise model is given by

$$\begin{aligned} \sigma^2(\lambda_1,\lambda_2) &= \sigma_L^2 \left(\frac{1-\tanh\left(\alpha(\lambda_2 - p_C(\lambda_1))\right)}{2} \right)^2 + \sigma_R^2 \left(\frac{1+\tanh\left(\alpha(\lambda_2 - p_C(\lambda_1))\right)}{2} \right)^2 + \\ &+ \left(\frac{\beta}{\cosh^2\left(\alpha(\lambda_2 - p_C(\lambda_1))\right)} \right)^2, \end{aligned} \tag{3.4}$$

The last term in (3.4) is included to account for the fact that the simplif ed model (3.3) is expected to lead to larger errors near the discontinuity location. This extra error term is obtained from the derivative of the hyperbolic tangent function, i.e. from the inverse-squared hyperbolic cosine function. Figure 3.1 illustrates the form of both model function and the noise term in a simpler, one-dimensional setting where the discontinuity is characterized by a single constant.

The simplif ed model $g(\lambda_1,\lambda_2)$ and the noise model $\sigma^2(\lambda_1,\lambda_2)$ are parameterized by the coeff - cients c of the discontinuity polynomial, as well as by the *hyperparameter* set $h = (m_L, \sigma_L, m_R, \sigma_R, \alpha, \beta)$. In principle, the model $g(\lambda_1,\lambda_2)$ does not have real predictive power, we are merely interested in the values of the model parameter vector c, and any joint distribution over (c,h) will be marginalized with respect to hyperparameters h.

In the absence of additional information, we choose a uniform prior on the polynomial coeff cient vector c, i.e., $P(\mathcal{M}) = P(c) = 1/\Delta^{K+1} = \text{const}$ on a hypercube $[-\Delta/2, +\Delta/2]^{K+1}$ for suff ciently large Δ. Uniform, positive-valued priors are also chosen for all hyperparameters.

The likelihood function $L(\mathcal{M}_C)$ is the probability of having the particular data set $\mathcal{D} = \{z_1,\ldots,z_N\}$ *if* it was drawn from Model $\mathcal{M}_C$ with coeff cients c and hyperparameters h. In terms of the log-likelihood,

$$\begin{aligned} \log P(\mathcal{D}|\mathcal{M}_C) = \sum_{i=1}^{N} \log\left(P(z_i|\mathcal{M}_C)\right) = \\ = -\sum_{i=1}^{N} \frac{(z_i - g(\lambda_1,\lambda_2))^2}{2\sigma^2(\lambda_1,\lambda_2)^2}. \end{aligned} \tag{3.5}$$

Given the likelihood $P(\mathcal{D}|\mathcal{M})$ and the prior $P(\mathcal{M})$, we then draw samples from the posterior distribution $P(\mathcal{M}|\mathcal{D}) \propto P(\mathcal{D}|\mathcal{M})P(\mathcal{M})$ via Markov Chain Monte Carlo (MCMC) sampling. MCMC is a class of techniques that allows sampling from a posterior distribution by constructing

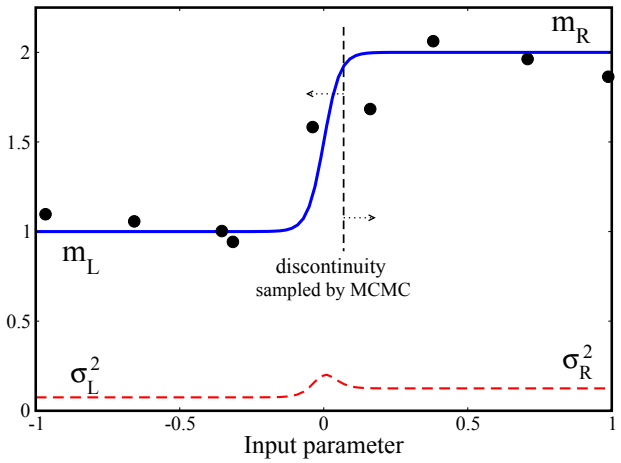

Figure 3.1. Illustration of the discontinuity detection algorithm for a one-parameter case. The blue curve corresponds to the simplif ed model $\mathcal{M}$, while black dots represent Data $\mathcal{D}$. The shape of noise model is illustrated by the red dashed line.

a Markov Chain that has the posterior as its stationary distribution [7, 11]. In particular, we are using the adaptive Metropolis algorithm [12]. This methodology is an improvement over the original Metropolis algorithm [19], since it uses the covariance of the previously visited chain states to f nd better proposal directions, thus exploring the posterior distribution in a more eff cient manner by accounting for the correlations between the parameters; see [12] for details.

The outcome of the MCMC chain is a distribution over the space of possible discontinuity curves. Specif cally, we have a set of sample parameter vectors c, each corresponding to a discontinuity curve. Whenever there is a need to emphasize the stochasticity of these curves and their corresponding parameter sets, we will use the argument ω as an element of the sample space of the MCMC chain to write the discontinuity curve as

$$p_C(x;\omega) = \sum_{k=0}^{K} c_k(\omega)x^k. \tag{3.6}$$

Since the "true" discontinuity $G(\lambda_1,\lambda_2) = 0$ is not known exactly, the posterior distrbutions for the above coeff cients will be used to generate samples for possible discontinuity locations and partition the parameter space into regions where the model Z varies smoothly.

Numerical tests

Here and further in this work, we demonstrate the methodology on test cases with artif cially generated data. We generated a synthetic discontinuous data set $z_1, \ldots, z_N$ by evaluating a bivariate error function with discontinuity strength parameter γ, discontinuity curve $\lambda_2 = r(\lambda_1)$, and an additional global oscillatory structure with amplitude δ

$$z_i = \frac{3}{2} + \frac{1}{2}\,\mathrm{erf}\left(\gamma(\lambda_{2i} - r(\lambda_{1i}))\right) + \delta \sin\left(\frac{\pi}{3}(\lambda_{1i} + \lambda_{2i})\right) \tag{3.7}$$

at points $\{\lambda_1, \ldots, \lambda_N\} = \{(\lambda_{1i}, \lambda_{2i})\}_{i=1}^{N}$.

First, let us demonstrate how the discontinuity detection algorithm works in a very simple setting, where the true answer is intuitively clear. Namely, assume data is given at a uniform 7×7 grid, and the true discontinuity is along the horizontal line $\lambda_2 = r(\lambda_1) = 0.3$. The steepness parameter is set to a very large value, $\gamma = 10^5$, and the last term in (3.7) is set to zero (i.e. $\delta = 0$). Hence, the data values are $z_i = 2$ if $\lambda_{2i} \geq 1/3$ and $z_i = 1$ if $\lambda_{2i} \leq 0$, although the true threshold is at $\lambda_2 = 0.3$, see Figure 3.2a). Clearly, any curve that is in the 'gap' $[0, 1/3]$ is an equally good answer for the discontinuity location. Let us look for a linear discontinuity $\lambda_2 = c_0 + c_1\lambda_1$. A simple computation suggests that all the lines that are inside the 'gap' must satisfy slope-intercept inequalities:

$$\begin{aligned} 0 &< c_0 + c_1 < 1/3, \\ 0 &< c_0 - c_1 < 1/3. \end{aligned} \tag{3.8}$$

Note that the locus of such points (c_0, c_1) is a rhombus with a center at $(1/6, 0)$.

In order to obtain a well-behaved Markov chain in this simple test case, we do not infer the steepness α. Instead, this parameter is set to the true value, i.e. $\alpha = 100000$. Figure 3.2(a) shows the data values and some samples of discontinuity lines taken from the stationary state of the Markov chain, while Figure 3.2(b) shows the values of the Markov chain for the parameters c_0 and c_1 in the stationary regime, i.e. after an initial, burn-in period is thrown away. Clearly, the parameters fall inside the "true" answer, i.e. the rhombus region in Fig. (3.2). Each point in the (c_0, c_1) space corresponds to a line, and they fall into the "gap" where the discontinuity is expected. In fact, all discontinuity lines are equally likely, and MCMC clearly samples from a uniform distribution with a rhombus-shaped support. The joint-posterior density of the polynomial coeff cients is shown in Figure 3.2(c). This example not only shows that the algorithm is leading to an expected answer, but also illustrates the need for having a probabilistic representation for the discontinuity location, given only limited number of samples.

Let us consider another, slightly more involved, example. The input parameter space is now $[0.5, 6] \times [0, 2]$, while the discontinuity curve is an inverse function that goes through $(2, 2)$ and $(5, 0)$, i.e. $\lambda_2 = r(\lambda_1) = \frac{20}{3}\left(\frac{1}{\lambda_1} - \frac{1}{5}\right)$. The amplitude of the additional structure is set to $\delta = 0.1$, and the steepness parameter is $\gamma = 2$.

Figure 3.3 illustrates the linear and quadratic (i.e., $K = 1$ and $K = 2$) discontinuity detection results for $N = 20$ and $N = 100$ input data points. The values of the forward function z_i evaluated

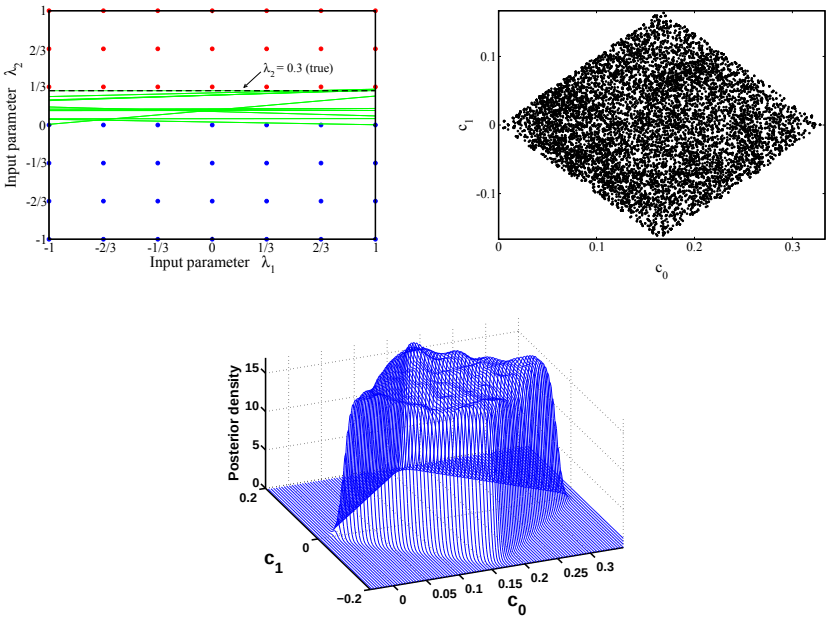

Figure 3.2. Illustration of the discontinuity detection algorithm. (a) The input parameters at a uniform grid with the output response color-coded as high (red) and low (blue), together with the exact discontinuity line $\lambda_2 = 0.3$ (black dashed line) and ten discontinuity lines sampled from the posterior distribution with MCMC (green lines), (b) the MCMC samples in the convergent regime: each point corresponds to a sample discontinuity line, (c) the joint posterior density of the slope and intercept of the discontinuity lines: the true answer is recovered, i.e. uniform distribution on a rhombus-shaped support.

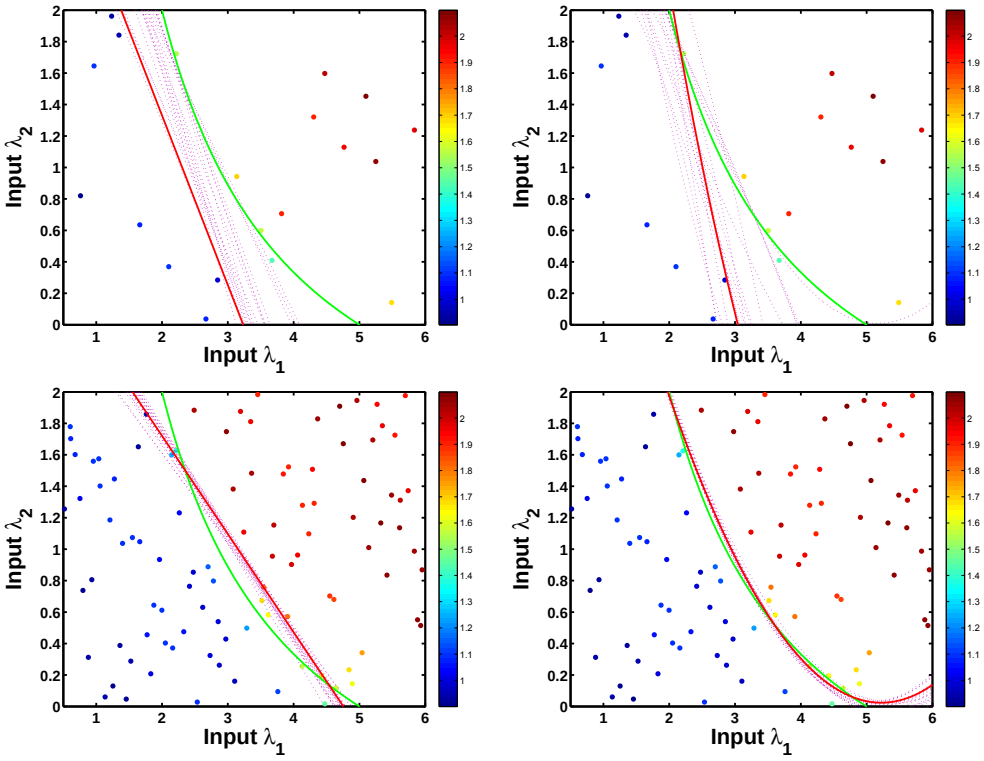

Figure 3.3. A test case with a discontinuity curve $\lambda_2 = 1/\lambda_1$. Top row: $N = 20$ input data points. Bottom row: $N = 100$ input data points. Left column: linear discontinuity inference ($K = 1$). Right column: quadratic discontinuity inference ($K = 2$). The colorbar corresponds to the output values z_i. The green line is the true discontinuity curve, the red line is the MAP estimate, and the dashed purple lines are samples drawn from the posterior distribution.

at input parameter points $(\lambda_{1i}, \lambda_{2i})$ are color-coded. The true discontinuity curve is also plotted along with the MAP estimate of the discontinuity and several samples of the discontinuity taken from the posterior distribution. Clearly, even linear discontinuity inference leads to reasonable approximation of the location of the discontinuity with sample curves spanning the true discontinuity region. Nevertheless, with large number of sample points, see the bottom row in Figure 3.3, the quadratic discontinuity inference improves the answer considerably. In most situations, however, there is no information about the structure of the discontinuity, and the probabilistic representation of the linear approximation spanning the true discontinuity location turns out satisfactory.

This page intentionally left blank.

Chapter 4

Global Polynomial Chaos expansions

We will use Polynomial Chaos (PC) expansions to represent the uncertain input parameters λ_1 and λ_2 as random variables with probability distribution functions. Specif cally, we will use Legendre-Uniform PC expansions (PCEs), that are well-suited when dealing with input parameters on compact domains. For convenience, we will assume the uncertain parameters λ_1 and λ_2 to be independent. The methodology would not suffer if the model parameters were jointly distributed.

PCEs (4.1) will used to represent the uncertainty in the input parameters in terms of independent Uniform $[0,1]$ random variables η_1 and η_2, Legendre polynomials $\Psi_k^{(1)}(\cdot)$ (rescaled to the domain $[0,1]$ for convenience) and deterministic *PC modes* μ_{1k}, μ_{2k}.

$$\begin{aligned} \lambda_1 &= \textstyle\sum_{k=0}^{P} \mu_{1k} \Psi_k^{(1)}(\eta_1) = F_{\lambda_1}^{-1}(\eta_1), \\ \lambda_2 &= \textstyle\sum_{k=0}^{P} \mu_{2k} \Psi_k^{(1)}(\eta_2) = F_{\lambda_2}^{-1}(\eta_2) \end{aligned} \tag{4.1}$$

The superscripts are used to denote the number of arguments of polynomials, i.e. $\Psi^{(i)}(\cdot)$ is an i-variate Legendre polynomial. A one-to-one correspondence between η_1 and λ_1, as well as between η_2 and λ_2 can be realized, say, through the respective inverse cumulative distribution functions $F_{\lambda_1}^{-1}$ and $F_{\lambda_2}^{-1}$. Next, we express the forward model output as a PC expansion of order p_{ord} in terms of bivariate Legendre polynomials $\Psi_p^{(2)}(\cdot,\cdot)$ and the random variable pair $(\eta_1,\eta_2) = (F_{\lambda_1}(\lambda_1), F_{\lambda_2}(\lambda_2))$ that is related to the two uncertain parameters through their cumulative distribution functions. Specif cally, the output function $Z(\lambda_1,\lambda_2)$ can be written as

$$Z(\lambda_1,\lambda_2) = Z(F_{\lambda_1}^{-1}(\eta_1), F_{\lambda_2}^{-1}(\eta_2)) \equiv \tilde{Z}(\eta_1,\eta_2) = \sum_{p=0}^{P} Z_p \Psi_p^{(2)}(\eta_1,\eta_2), \tag{4.2}$$

up to bivariate polynomial order p_{ord}, with the number of terms $P+1 = (p_{\text{ord}}+2)(p_{\text{ord}}+1)/2$. In order to obtain PC coeff cients Z_p, we will employ two different methods, orthogonal projection and Bayesian inference.

Orthogonal projection

The orthogonal projection relies on the orthogonality of the basis functions leading to the Fourier-like formulas

$$Z_p = \frac{\langle \tilde{Z}(\eta_1,\eta_2)\Psi_p^{(2)}(\eta_1,\eta_2)\rangle}{\langle \Psi_p^{(2)}(\eta_1,\eta_2)\Psi_p^{(2)}(\eta_1,\eta_2)\rangle}. \tag{4.3}$$

The expectation $\langle\cdot\rangle$ is taken with respect to the probability distribution of the variables (η_1,η_2), which conveniently is a constant on $[0,1]$ in the Legendre-Uniform case. The denominator of (4.3) is precomputed, while the numerator expectation is typically calculated through a quadrature rule

$$\begin{aligned}
\langle \tilde{Z}(\eta_1,\eta_2)\Psi_p^{(2)}(\eta_1,\eta_2)\rangle &= \int_{[0,1]^2} \tilde{Z}(\eta_1,\eta_2)\Psi_p^{(2)}(\eta_1,\eta_2)d\eta_1 d\eta_2 \\
&\approx \sum_{q=1}^{N_q} \tilde{Z}(\eta_1^{(q)},\eta_2^{(q)})\Psi_p^{(2)}(\eta_1^{(q)},\eta_2^{(q)})w^{(q)} \\
&= \sum_{q=1}^{N_q} Z(F_{\lambda_1}^{-1}(\eta_1^{(q)}),F_{\lambda_2}^{-1}(\eta_2^{(q)}))\Psi_p^{(2)}(\eta_1^{(q)},\eta_2^{(q)})w^{(q)},
\end{aligned} \tag{4.4}$$

requiring the evaluation of the forward model $z^{(q)} = Z(\lambda_1^{(q)},\lambda_2^{(q)})$ at the locations corresponding to quadrature points, i.e., at $(\lambda_1^{(q)},\lambda_2^{(q)}) = (F_{\lambda_1}^{-1}(\eta_1^{(q)}),F_{\lambda_2}^{-1}(\eta_2^{(q)}))$. Here $w^{(q)}$ are the weights associated with the quadrature rule.

Bayesian inference

The Bayesian inference approach, although computationally more intensive, is able to obtain a PC representation with associated uncertainties given limited number of forward model runs that can be distributed arbitrarily in the input parameter space. Specif cally, the Bayes' formula

$$P(\mathcal{M}\,|\mathcal{D}) = \frac{P(\mathcal{D}\,|\mathcal{M}\,)P(\mathcal{M}\,)}{P(\mathcal{D}\,)} \tag{4.5}$$

is applied with the vector of PC coeff cients $Z = (Z_0,\ldots,Z_p)$ as the Model $\mathcal{M}_Z$. The forward model outputs $z^{(b)} = Z(\lambda_1^{(b)},\lambda_2^{(b)})$, which correspond to PC input parameters via CDF maps $\eta_1 = F_{\lambda_1}(\lambda_1)$ and $\eta_2 = F_{\lambda_2}(\lambda_2)$ for $b = 1,\ldots,N_b$, are considered as Data $\mathcal{D}$. A simple, gaussian noise model with constant variance σ^2 across the parameter range is assumed in order to obtain the log-likelihood function

$$\begin{aligned}
\log P(\mathcal{D}\,|\mathcal{M}_Z) &= \sum_{b=1}^{N_b} \log\left(P(z^{(b)}|\mathcal{M}_Z)\right) \\
&= -\sum_{b=1}^{N} \frac{\left(z^{(b)} - \sum_{p=0}^{P} Z_p \Psi_p^{(2)}(F_{\lambda_1}(\lambda_1^{(b)}),F_{\lambda_2}(\lambda_2^{(b)}))\right)^2}{2\sigma^2}.
\end{aligned} \tag{4.6}$$

Again, the adaptive MCMC algorithm is employed [19, 12], and we will primarily be interested in the maximum a posteriori (MAP) estimate of the model parameters, i.e. PC modes, $(Z_0, \ldots, Z_P)$.

Note that, unlike the quadrature projection case, there are no restrictions to the location of the points where the forward model is evaluated, i.e. the pairs $(\lambda_1^{(b)}, \lambda_2^{(b)})$ can be arbitrarily distributed in the input parameter space. Although the quadrature projection approach described in Section 4 has low computational cost and it also leads to an optimal representation in the L_2-sense [9], the Bayesian inference approach is sometimes more suitable due to its ability to obtain a reasonable representation with limited and arbitrarily distributed input parameters.

Failure of global expansions

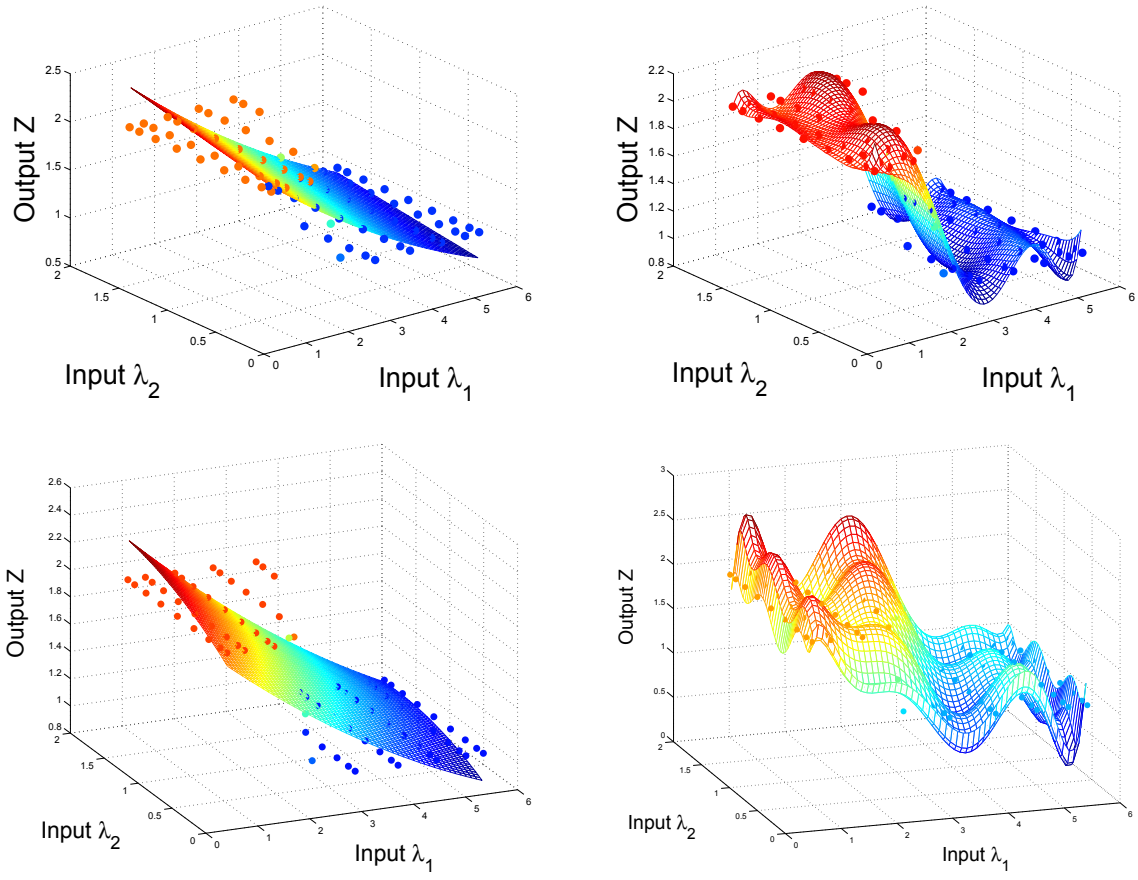

Figure 4.1. Top: orthogonal projection, Bottom row: Bayesian inference (MAP). Left: order 2, Right: order 7.

In both quadrature projection and Bayesian inference approaches, the spectral representation

(4.2) assumes a certain degree of smoothness in the output Z with respect to its arguments (λ_1, λ_2). For example, in the Meridional Overturning Circulation case, outlined in Section 2, the maximum overturning stream function undergoes a bifurcation with respect to the climate sensitivity λ (lbd_1) and the rate of CO_2 increase r (λ_2), essentially making the use of the global expansion (4.2) infeasible. Figure 4.1 demonstrates how the global PC expansion fails to properly represent discontinuous data sets. Lower order expansions do not capture the global behavior well, while higher order expansions exhibit Gibbs phenomenon, i.e. non-physical oscillations. In this simple example, uniform input parameters are taken, i.e. $\lambda_1 = \eta_1$ and $\lambda_2 = \eta_2$, to enable an easy orthogonal projection (4.3) via quadrature integration.

In principle, multi-domain PC expansions [13, 15, 16, 23] allow local representations that effectively overcome this issue. However, these local representations are strongly challenged by the computational cost of running the forward model at the quadrature point locations for each subdomain, since they are generally computed by adaptive ref nement of domains with new data samples required for each level of ref nement. We propose a methodology that essentially builds a smarter domain decomposition algorithm, taking advantage of the fact that there is a single discontinuity curve. The state of knowledge of the location of the discontinuity curve is represented by the distribution of its samples, obtained by Bayesian inference described in Section 3.

The knowledge of the discontinuity location suggests that separate PC expansions for the output Z on each side of the discontinuity could lead to more accurate representations compared to global PC expansions. Essentially, this corresponds to a 'smart' domain decomposition, where domain is not split by half on each dimension, rather it is split according to the discontinuity location. However, compact-support PC representations require rectangular domains and are not readily applicable to the resulting irregular domains on either side of the discontinuity curve. For this reason we will employ a domain mapping strategy outlined next.

Chapter 5

Polynomial Chaos Representation via Parameter Domain Mapping

PC representation for a fixed discontinuity curve

For each sample discontinuity curve $\lambda_2 = p_C(\lambda_1;\omega)$ we find maps from irregular parameter domains (λ_1,λ_2) on either side of the discontinuity curve to rectangular domains (η_1',η_2') via the Rosenblatt transformation [22]. Namely, assume the discontinuity curve $\lambda_2 = p_C(\lambda_1;\omega)$ divides the full rectangular domain $D = I_{\lambda_1} \times I_{\lambda_2}$ into two subdomains D_L and D_R. Note that on each side of the discontinuity, λ_1 and λ_2 are not independent anymore; the dependency is enforced by the domain boundary $\lambda_2 = p_C(\lambda_1;\omega)$. The inverse of the Rosenblatt transformation

$$\begin{aligned} \lambda_1 &= \tilde{F}_{\lambda_1}^{-1}(\eta_1^L), \\ \lambda_2 &= \tilde{F}_{\lambda_2|\lambda_1}^{-1}(\eta_2^L|\eta_1^L) \end{aligned} \tag{5.1}$$

maps the regular *stochastic* domain $[0,1]\times[0,1]$ to the left *parametric* domain D_L and uses the inverses of the marginal and conditional cumulative distribution functions for the random variable pair (λ_1,λ_2) restricted to the left domain only. To be precise, the joint distribution of the input parameter on the left of the discontinuity curve is

$$\tilde{F}(x,y) = P(\lambda_1 < x, \lambda_2 < y | (\lambda_1,\lambda_2) \in D_L) \tag{5.2}$$

The right domain is treated in the same way. Throughout this work we use densities for the uncertain parameters λ_1 and λ_2, shown in Figure 5.1, taken from the MOC context described in Chapter 2. Namely, we take two climate model input parameters, climate sensitivity λ and the rate of CO_2 increase r with probability density functions that are found from historical records and from expert opinions [30]. For the purposes of this work, these parameters are assumed independent without restricting the generality of the described methodologies. However, note that after constraining to left or right domains only in (5.2), the input parameters become dependent.

The map from (η_1^L,η_2^L) to (λ_1,λ_2) helps obtain a well-defined PC representation

$$Z_C^L(\lambda_1,\lambda_2) = \tilde{Z}_C^L(\eta_1^L,\eta_2^L) = \sum_{p=0}^{P} z_p^L \Psi_p^{(2)}(\eta_1^L,\eta_2^L) \tag{5.3}$$

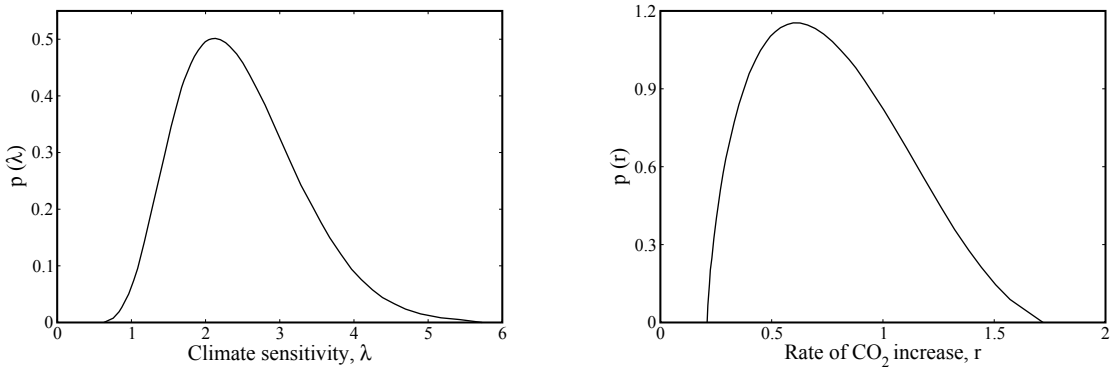

Figure 5.1. Probability density functions for λ_1 (climate sensitivity) and λ_2 (CO_2 rate of increase) that represent the input parameters of the forward model.

for the output on the left domain either using Galerkin projection

$$z_p^L = \frac{\langle \tilde{Z}(\eta_1^L, \eta_2^L)\Psi_p^{(2)}(\eta_1^L, \eta_2^L)\rangle}{\langle \Psi_p^{(2)}(\eta_1^L, \eta_2^L)\Psi_p^{(2)}(\eta_1^L, \eta_2^L)\rangle} \tag{5.4}$$

or Bayesian inference methodology outlined in Section 4.

Figure 5.2(a) shows sample domain mappings for one instance of discontinuity line for the orthogonal projection approach. In the stochastic domains (η_1, η_2) a total of M_q^2 quadrature points are generated to enable the orthogonal projection (5.4) for D_L and D_R. For each instance of the discontinuity curve, there is a set of points on each side of the parametric domain (D_L and D_R) corresponding to these quadrature points. In order to evaluate the integrals in (5.4), the forward model needs to be sampled in the parametric domain at these $2M_q^2$ locations. In contrast with the projection approach, the inference approach is driven by the parametric domain points. As can be seen in Figure 5.2(b), the points in the parametric domain can be unchanged, i.e. one can reuse the same forward model runs that were employed to detect the discontinuity. This approach leads to points in the stochastic domain (η_1, η_2) that are in principle arbitrarily distributed. Bayesian inference of PC on each side of the discontinuity is potentially less precise and more expensive than the quadrature integration approach, but it does not require any new forward model runs. We advocate for the use of a *hybrid* approach. Namely, in order to have a reasonable sample coverage in the stochastic domain, one set of quadrature points is picked at each side of the MAP estimate of the discontinuity. Further, the preimages of these quadrature points are added to the set of points in the parametric domain, i.e. extra $2M_q^2$ points, just like in the first approach above. These data samples will be reused for all discontinuity curve samples, using Bayesian inference approach, since the data set for general (other then the MAP estimate) discontinuities will not map to a quadrature locations in the stochastic domain anymore. Figure 5.2(c) illustrates the domain mapping and the points' locations in the hybrid approach.

Having obtained PC expansions for the output response on both sides of the discontinuity separately, we def ne the global response representation for a f xed discontinuity curve c in the following way:

$$Z_c(\lambda_1,\lambda_2) = \begin{cases} Z_c^L(\lambda_1,\lambda_2) & \text{if } (\lambda_1,\lambda_2) \in D_L \\ Z_c^R(\lambda_1,\lambda_2) & \text{if } (\lambda_1,\lambda_2) \in D_R \end{cases}. \tag{5.5}$$

Averaging expansions over sample curves

To this end we obtained a "piecewise-spectral" representation (5.5) for the response function $Z_c(\lambda_1,\lambda_2)$ for a f xed discontinuity curve that is parameterized by its coeff cients c. However, the Bayesian methodology in Chapter 3 offers a framework to obtain the full uncertainty in these curves. Therefore, we can obtain the expectation of the representation $Z_c(\lambda_1,\lambda_2)$ with respect to the multidimensional posterior probability distribution function $p(c)$ of the coeff cient vector c:

$$\hat{Z}(\lambda_1,\lambda_2) = \int_C p(c) Z_c(\lambda_1,\lambda_2) dc. \tag{5.6}$$

The integral in (5.6) is too expensive to compute with Monte Carlo sampling, although the samples are available from the discontinuity detection MCMC. Indeed, the Monte Carlo integration would involve two PC projections $Z_c^{L,R}(\lambda_1,\lambda_2)$ for each sample curve c. Moreover, there is no direct way to f nd the domain C of the integration either - only samples drawn from the distribution $p(c)$ are available. Once again, we will use the Rosenblatt transformation $\eta = R(c)$ to map the unknown domain of integration C to a rectangular domain $[0,1]^{K+1}$. The vector of random variables u def ned with the help of the conditional distributions of c

$$\begin{aligned} u_0 &= F_0(c_0), \\ u_1 &= F_{1|0}(c_1|c_0), \\ &\dots \\ u_K &= F_{K|K-1,\dots,0}(c_K|c_{K-1},\dots,c_0) \end{aligned} \tag{5.7}$$

has independent Uniform[0,1]-distributed components. The integral in (5.6) can be then rewritten as

$$\hat{Z}(\lambda_1,\lambda_2) = \int_{[0,1]^{K+1}} Z_{R^{-1}(u)}(\lambda_1,\lambda_2) du. \tag{5.8}$$

The latter integral is computed by quadrature rule

$$\hat{Z}(\lambda_1,\lambda_2) \approx \sum_{u^*} Z_{R^{-1}(u^*)}(\lambda_1,\lambda_2) w^*. \tag{5.9}$$

The Rosenblatt transformation in (5.7) relies on the joint cumulative distribution function $F(c_K,\dots,c_1,c_0)$, which is estimated based on the samples provided by MCMC via Kernel Density Estimation (KDE) [25, 27]. In order to accurately capture the multidimensional distribution, one needs sample it at a rate that increases exponentially as the dimensionality $K+1$ grows, hence the Rosenblatt transformation (5.7) suffers from the curse of dimensionality. Note that this is not an issue in (5.1),

since in that implementation of the Rosenblatt transformation we have access to the PDF itself, not just samples of it.

Since the structure of the discontinuity curve is *a priori* unknown, and to make the sampling-based Rosenblatt transformation feasible, we infer a linear discontinuity curve (i.e., $K = 1$). The results in the next section illustrate that averaging over these low-order auxiliary curves by (5.6) improves the overall accuracy, and leads to a smooth global representation of the model output $Z(\lambda_1, \lambda_2)$.

Assume that a total of N_q^2 quadrature points are used in order to compute the average representation (5.9). Each of these quadrature points, shown with f lled circles in Figure 5.4b), corresponds to a discontinuity curve. According to Section 5, for each discontinuity curve, a total of $2M_q^2$ forward model runs are required for the orthogonal projection. This leads to a total of $2M_q^2 N_q^2$ forward model runs. Indeed, Figure 5.3 shows the distribution of the preimages of quadrature points in the stochastic domain, i.e. the points where the forward model needs to be simulated. In this case, we used $M_q = N_q = 5$ points per dimension for both the orthogonal projection at each side of the discontinuity and for integrating in the discontinuity curve space. Therefore, the orthogonal projection approach would require 1250 extra evaluations for the forward model. While this could be acceptable for forward models with moderate computational cost per simulation, it becomes a considerable handicap for highly complex forward models, such as global climate models of high grid resolution and complexity. For such applications, the Bayesian strategy of inferring PC expansions at each sides of discontinuity is much better suited, since it relies on the original set of points in the parametric domain without any restrictions as to where these points would map in the stochastic domain. The Bayesian inference therefore will be less precise in approximating the forward model due to both lower number of sampling points and their irregular locations, but it can be the only alternative when the forward model runs are very expensive or even impossible. The hybrid approach in some sense hedges and provides a combination of the advantages of orthogonal projection and Bayesian inference. Namely, one chooses quadrature points' preimages (under the Rosenblatt transformation) in the parametric domain for the MAP value of the discontinuity only, and then proceeds with the inference approach. This would ensure that the stochastic domain is covered reasonably well for the rest of the discontinuity curves, requiring only $2M_q^2$ extra forward model runs, see Figure 5.2c).

Uncertainty Propagation via Parameter Domain Mapping

In this section we demonstrate the full algorithm of discontinuity detection and response surface approximation, together with uncertainty propagation from input parameter distributions to output distribution. Consider now a synthetic forward model 3.7, with a steepness parameter $\gamma = 2$, a discontinuity along a cubic curve $\lambda_2 = r(\lambda_1) = 1 + (\lambda_1 - 3)^3$ and additional oscillatory structure of amplitude $\delta = 0.1$.

Figure 5.4(a) illustrates the inference of the discontinuity curve, the true location of which is shown with thick green line. Since the true discontinuity is set to a third order polynomial, its

shape that cannot be approximated by a single straight line. However, the MCMC chain provides an ensemble of lines which cover the region of sharp gradients, i.e. where the model output varies sharply between high (red symbols) and low (blue symbols) values.

It is worth noting that the random vector c has dependent components. As an example, Figure 5.4(b) shows the contours of joint posteriors of the curve parameters c_0 and c_1, as well as the quadrature points $R^{-1}(u^*)$ generated by the inverse Rosenblatt transformation to enable integration in the (c_0, c_1) space, see Eqs. (5.6)-(5.9).

Figure 5.5 shows a comparison between the synthetic model and the values obtained using the averaged PC expansion (5.6) with both quadrature approach and Bayesian inference. Despite the challenge posed by the relatively wide regions with f at z-values, the averaged PC expansion $\hat{Z}(\lambda_1, \lambda_2)$ captures well the steep gradients of the synthetic model. Overall, the quadrature approach works slightly better. The orthogonal projection requires $2M_q^2 N_q^2$ extra forward model runs to obtain PC expansions on each sides of he discontinuity, while the Bayesian inference relies on the same forward model runs that were used to f nd the discontinuity location in the f rst place.

Having the averaged PC expansion as a surrogate representation of the input-output relationship, one can also perform uncertainty propagation from input parameter distributions to the output distribution by simple Monte Carlo sampling. Figure 5.6 illustrates the distribution of the output response based on the true model, as well as averaged PC expansions using both orthogonal projection and Bayesian inference approach. The values of PDF obtained through the averaged PC expansion (5.6) are in good quantitative agreement with the ones obtained from the full model (3.7). These plots illustrate the accomplishment of the basic uncertainty propagation task: given the PDFs of the parameter pair (λ_1, λ_2), obtain the PDF of the output representation with limited forward model evaluations.

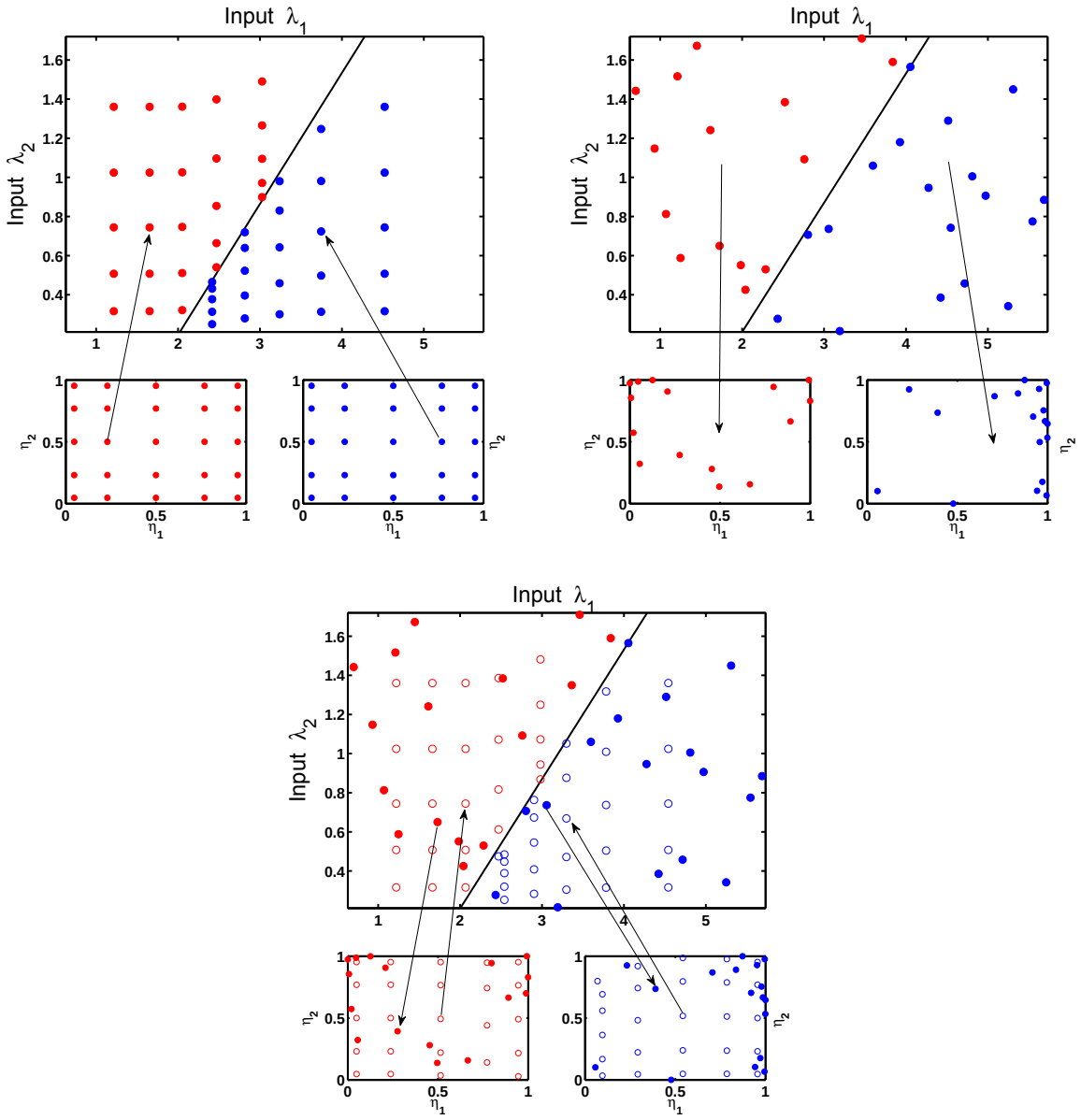

Figure 5.2. Sample domain mappings through Rosenblatt transformation between parametric and stochastic domains. The discontinuity curve is shown with a black line. (a) The orthogonal projection-based approach relies on the stochastic domain quadrature points and maps back to the parametric domain, while (b) the Bayesian inference approach uses the input data at hand from parametric domain and maps it to the stochastic domain, and, f nally, (c) the hybrid approach incorporates both methods to ensure better spread of points in the stochastic domain. The empty circles represent the quadrature points and their preimages in this case.

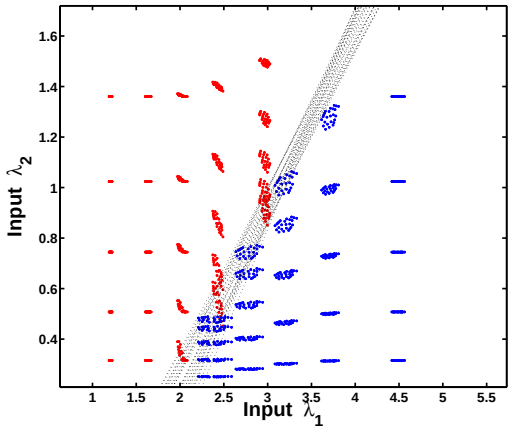

Figure 5.3. The extra points in the parametric domain where new forward model runs are required in order to obtain a projection-based response surface. We used $M_q = 5$ points per dimension for orthogonal projection on each side of the discontinuity. The averaging with respect to the discontinuity curves has been taken via quadrature integration with $N_q = 5$ points per dimension, a total of 25 discontinuity curves, marked with black dotted lines. This leads to $2M_q^2N_q^2 = 1250$ new points where the forward model needs to be evaluated.

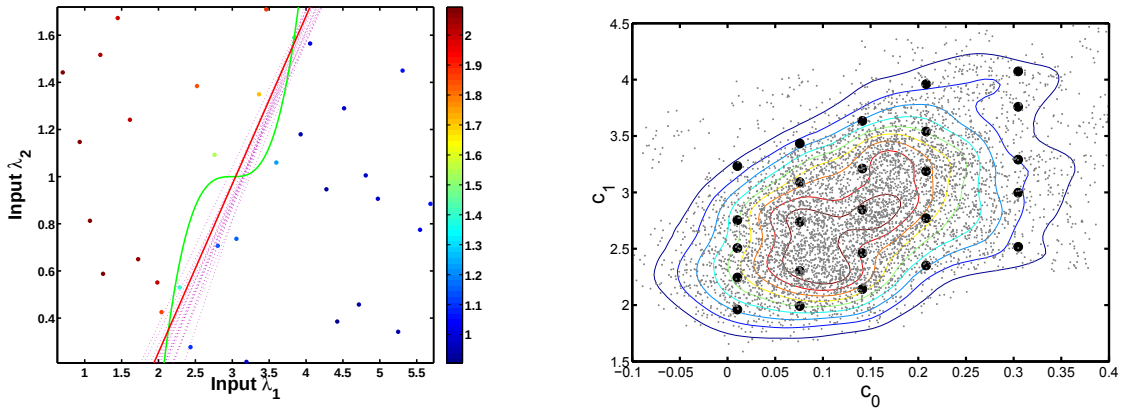

Figure 5.4. (a) Sample discontinuity lines (dashed purple lines) obtained through Bayesian inference. The thick red line is the MAP estimate of the discontinuity. The thick green line corresponds to the true discontinuity $r(\lambda_1) = 1 + (\lambda_1 - 3)^3$. Data samples are color-coded according to the synthetic model output (3.7). (b) Joint posterior distribution of components c_0 and c_1 of the random vector c. The filled circles are the quadrature points used in (5.6). Small dots are samples from the Markov chain. The number of original sample points is set to $N = 33$.

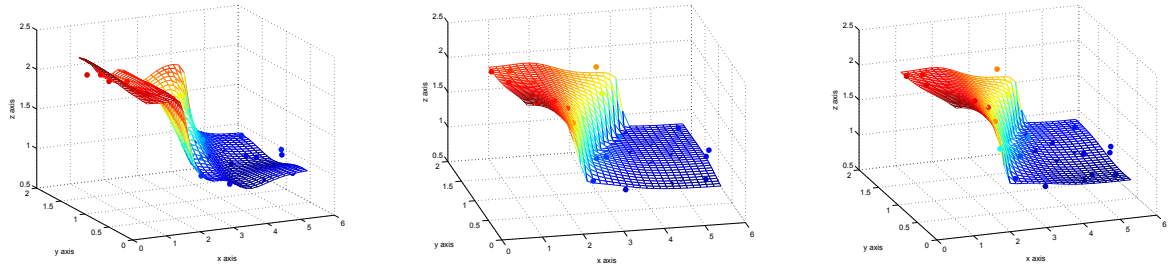

Figure 5.5. The Averaged-PC expansion surface $\hat{Z}(\lambda_1, \lambda_2)$ fits the original discontinuous samples. The PC expansions on each side of the sampled discontinuty are obtained by (a) quadrature projection, (b) Bayesian inference.

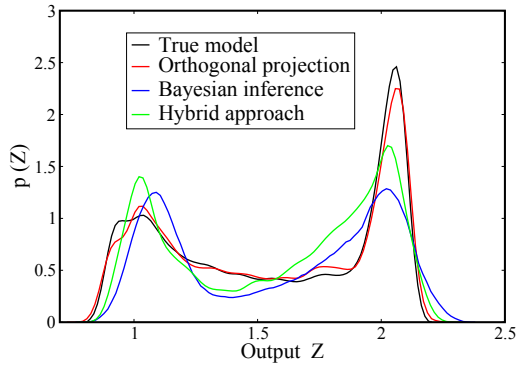

Figure 5.6. Comparison of the distributions based on synthetic model and averaged PC expansions with both orthogonal projection and Bayesian inference employed for each side of the discontinuity.

This page intentionally left blank.

Chapter 6

Conclusions

In this report, we present a methodology for uncertainty quantification in models with limited data and discontinuities. The underlying assumptions are (a) there is only limited data available or limited capacity to obtain new data, i.e. forward model runs are expensive enough to render brute-force domain decomposition algorithms infeasible, and (b) the data exhibits discontinuities or steep gradients across a certain curve in the parameter region. We propose a Bayesian approach to detect and parameterize the discontinuities as well as the uncertainties associated with them. Next, we use a domain mapping strategy to map each irregular sub-domains to rectangular ones where the application of the local spectral methods of uncertainty propagation is feasible. Essentially, this methodology is a "smart" domain decomposition, where one first approximately finds the discontinuity location and then splits the domain accordingly.

The computation of PC expansion coefficients on each side of the discontinuity can be performed using either orthogonal projection or Bayesian inference methodologies. Orthogonal projection, although performs better, requires the forward model evaluation at the preimages of the quadrature points under the Rosenblatt transformation. This approach puts a restriction on the positions of the sampling points in the parametric domain (λ_1, λ_2). Moreover, for every sample of the discontinuity curve, new samples in the parametric domain would be needed. The Bayesian inference approach, on the other hand, allows obtaining a reasonable representation with the data available at hand, at the same time characterizing the uncertainties associated with the result. This approach is in general less precise, since it is driven by available points in the parametric domain that can in principle cover the stochastic, PC domain poorly. We propose a hybrid approach to balance between computational cost and accuracy of the resulting representation - the approach requires only one set of extra forward model runs in order to spread the points in the stochastic domain well. A more formal experimental design strategy to improve the accuracy of both the discontinuity location and the resulting PC representation is a matter of ongoing work.

This page intentionally left blank.

References

[1] R. Archibald, A. Gelb, R. Saxena, and D. Xiu. Discontinuity detection in multivariate space for stochastic simulations. *Journal of Computational Physics*, 228:2676–2689, 2009.

[2] R. Archibald, A. Gelb, and J. Yoon. Polynomial f tting for edge detection in irregularly sampled signals and images. *SIAM J. Numer. Anal.*, 43(1):259–279, 2005.

[3] M. Basu. Gaussian-based edge detection methods: a survey. *IEEE Transactions on Systems, Man, and Cybernetics, Part C*, 32(3):252–260, 2002.

[4] T. Chantrasmi, A. Doostan, and G. Iaccarino. Padé-legendre approximants for uncertainty analysis with discontinuous response surfaces. *J. Computat. Phys.*, 228(19):7159–7180, 2009.

[5] C. Daux, N. Moës, J. Dolbow, N. Sukumar, and T. Belytschko. Arbitrary branched and intersecting cracks with the extended f nite element method. *Int. J. Numer. Meth. Engng*, 48:1741–1760, 2000.

[6] M. Fleming, Y.A. Chu, B. Moran, and T. Belytschko. Arbitrary branched and intersecting cracks with the extended f nite element method. *Int. J. Numer. Meth. Engng*, 40:1483–1504, 1997.

[7] Dani Gamerman. *Markov Chain Monte Carlo: Stochastic Simulation for Bayesian Inference*. Chapman & Hall, London, 1997.

[8] A. Ganachaud and C. Wunsch. The oceanic meridional overturning circulation, mixing, bottom water formation and heat transport. *Nature*, 408:453–457, 2000.

[9] R.G. Ghanem and P.D. Spanos. *Stochastic Finite Elements: A Spectral Approach*. Springer Verlag, New York, 1991.

[10] D. Ghosh and R. Ghanem. Stochastic convergence acceleration through basis enrichment of polynomial chaos expansions. *Int. J. Numer. Meth. Engng*, 73:162–174, 2008.

[11] W. R. Gilks, S. Richardson, and D. J. Spiegelhalter. *Markov Chain Monte Carlo in Practice*. Chapman & Hall, London, 1996.

[12] H. Haario, E. Saksman, and J. Tamminen. An adaptive Metropolis algorithm. *Bernoulli*, 7:223–242, 2001.

[13] O.P. Le Maître, R.G. Ghanem, O.M. Knio, and H.N. Najm. Uncertainty propagation using Wiener-Haar expansions. *J. Comput. Phys.*, 197(1):28–57, 2004.

[14] O.P. Le Maître and O.M. Knio. *Spectral Methods for Uncertainty Quantification*. Springer, New York, NY, 2010.

[15] O.P. Le Maître, H.N. Najm, R.G. Ghanem, and O.M. Knio. Multi-resolution analysis of Wiener-type uncertainty propagation schemes. *J. Comput. Phys.*, 197:502–531, 2004.

[16] O.P. Le Maître, H.N. Najm, P.P. Pébay, R.G. Ghanem, and O.M. Knio. Multi-resolution-analysis scheme for uncertainty quantif cation in chemical systems. *SIAM J. Sci. Comput.*, 29(2):864–889, 2007.

[17] O.P. Le Maître, M.T. Reagan, B.D. Debusschere, H.N. Najm, R.G. Ghanem, and O.M. Knio. Natural convection in a closed cavity under stochastic, non-Boussinesq conditions. *SIAM J. Sci. Comp.*, 26(2):375–394, 2004.

[18] J. F. McManus, R. Francois, J. M. Gherardi, L. D. Keigwin, and S. Brown-Leger. Collapse and rapid resumption of atlantic meridional circulation linked to deglacial climate changes. *Nature*, 428:834–837, 2004.

[19] N. Metropolis, A.W. Rosenbluth, M.N. Rosenbluth, A.H. Teller, and E. Teller. Equations of state calculations by fast computing machines. *J. Chem. Phys.*, 21(6):1087–1092, 1953.

[20] H.N. Najm, B.J. Debusschere, Y.M. Marzouk, S. Widmer, and O.P. Le Maître. Uncertainty Quantif cation in Chemical Systems. *Int. J. Num. Meth. Eng.*, 2008. in press.

[21] A. Nouy and A. Clement. eXtended Stochastic Finite Element Method for the numerical simulation of heterogenuous materials with random material interfaces. *Int. J. Numer. Meth. Engng*, 2010.

[22] M. Rosenblatt. Remarks on a multivariate transformation. *Annals of Mathematical Statistics*, 23(3):470 – 472, 1952.

[23] K. Sargsyan, B. Debusschere, H. Najm, and O. LeMaître. Spectral representation and reduced order modeling of the dynamics of stochastic reaction networks via adaptive data partitioning. *SIAM Journal on Scientific Computing*, 31(6):4395–4421, 2010.

[24] A. Schmittner and T. F. Stocker. The stability of the thermohaline circulation in global warming experiments. *Journal of Climate*, 12(4):1117–1133, 1999.

[25] D.W. Scott. *Multivariate Density Estimation. Theory, Practice and Visualization*. Wiley, New York, 1992.

[26] J. R. Scott, A. P. Sokolov, P. H. Stone, and M. D. Webster. Relative roles of climate sensitivity and forcing in def ning the ocean circulation response to climate change. *Climate Dynamics*, 30(5):441–454, 2008.

[27] B.W. Silverman. *Density Estimation*. Chapman and Hall, London, 1986.

[28] D.S. Sivia. *Data Analysis: A Bayesian Tutorial*. Oxford Science, 1996.

[29] M. Tatang, W. Pan, R. Prinn, and G. McRae. An eff cient method for parametric uncertainty analysis of numerical geophysical models. *J. Geophys. Res.*, 102:21925–21932, 1997.

[30] M.D. Webster, J. Scott, A. Sokolov, S. Dutkiewicz, and P. Stone. Estimating probability distributions from complex models with bifurcations: The case of ocean circulation collapse. *Journal of Environmental Systems*, 31(1):39–59, 2007.

[31] M.D. Webster and A.P. Sokolov. A Methodology for Quantifying Uncertainty in Climate Projections. *Climatic Change*, 46:417–446, 2000.

[32] D. Ziou and S. Tabbone. Edge detection techniques: an overview. *Int. J. Pattern Recognit. Image Anal.*, 8:537–559, 1998.

DISTRIBUTION:

1	MS 9051	Habib Najm, 8351
1	MS 9051	Bert Debusschere, 8351
1	MS 9051	Khachik Sargsyan, 8351
1	MS 9051	Cosmin Safta, 8954
1	MS 9155	Jerry McNeish, 8954
1	MS 9051	Damian Rouson, 8351
1	MS 9151	Jim Costa, 8950
1	MS 9054	Andrew McIlroy, 8350
1	MS 0754	Patrick Brady, 6730
1	MS 9004	William Ballard, 8100
1	MS 0899	Technical Library, 9536 (electronic copy)
1	MS 0123	D. Chavez, LDRD Off ce, 1011

Sandia National Laboratories